2022

Critical Impact of Fin Thermal Conductivity in the Modeling of Evaporator Under Frost Conditions

Antoine M. Parthoens

Samuel Gendebien

Vincent Lemort

Critical Impact of Fin Thermal Conductivity in the Modeling of Evaporator Under Frost Conditions

Antoine PARTHOENS[1], Samuel GENDEBIEN[1]*, Vincent LEMORT[1]

[1]Univesity of Liège, Thermodynamics Laboratory,
Liège, Belgium
a.parthoens@uliege.be
sgendebien@uliege.be
vincent.lemort@uliege.be

* Corresponding Author

ABSTRACT

Refrigeration systems such as heat pumps may be subject to frost formation. This phenomenon plays a major role in the heat pump overall performance drop due to the presence of an additional thermal resistance and an increase of the airside pressure drop. Deep experimental investigations show a typical pattern in frost distribution through the heat exchanger, in various operating conditions. A tube-by-tube simulation model is proposed. The dynamic model accounts for two-phase and overheated zones on the refrigerant side. On the air side, the frost may evolve independently on each tube and their corresponding fins, giving a non-uniform frost layer throughout the device. However, in a first time, important discrepancies are noticed between the distribution of frost predicted by the model and the obtained experimental data. The aforementioned model is then improved by taking the fin thermal conductivity into account. Unlike the first version of the model, the results from the new one match more closely with the experimental observations. This model is successfully validated by means of the empirical data. Such model can pave the way toward future designs of evaporator that requires accurate frost accretion prediction.

1. INTRODUCTION

Frost formation can be a major problem in heat exchangers and more particularly in heat pump evaporators. Under certain conditions, so-called frosting conditions, a frost layer can form on the heat exchanger surface. This frost layer leads to a reduction of the cross-section area. Obviously, this reduction then generates an increase in the pressure drop through the heat exchanger and thus an increase in the electrical power delivered to the fans (Tang et al. (2020)). If the electrical power delivered to the fans remains constant, the air flowrate flowing through the heat exchanger decreases (Chen et al., 2003). In extreme cases, the frost layer can create a full blockage of air flow passages (Xia et al. (2006)). Frost layer also corresponds to an additional thermal resistance that affects the exchanged heat transfer rate between the air stream and the refrigerant (Ye and Lee, 2013). As a consequence, the evaporator energy performance will be affected by the presence of frost and will ultimately decrease the performance of the heat pump. Yang et al. (2006) and Yoo et al. (2018) conducted experimental investigations to quantify the drop of heat transfer rate at the evaporator and the COP decrease of a heat pump, due to frost formation.

Many authors (Silva et al., 2011; Jiang et al., 2006; Kim et al., 2018; Mastrullo et al., 2014; Morales-Fuentes et al., 2018; Xia and Jacobi, 2017; Ye and Lee, 2018) developed different models of frost and of frost formation in the frame of heat exchanger devices. Basically, the more accurate the model, the more computational resource needed. However, as described in the present paper, relatively simple models with small computational time can lead to satisfying prediction results.

The modeling approach detailed in this paper consists in a tube-by-tube discretization, allowing to predict frost growth independently on each tube. A considerable add-on with respect to previous numerical investigations is the consideration of fin thermal conductivity in the model. Even if it is not a novelty in heat exchangers without frost apparition (Liu et al., 2004.; Romero-Méndez et al., 1997.; Sarfraz et al., 2019; Singh et al., 2003), from the best author's knowledge, it is a first time that this phenomenon is accounted in heat exchangers with frost formation. It is seen in the frame of this work that it has a capital importance in the frost distribution predictions.

2. EXPERIMENTAL INPUT

Experimentation is a key step to observe the different physical phenomena and to gather measurements and constitute a data base. A highly instrumented heat pump is built with, as the main objective, a special focus on the study of frost deposition in the evaporator. A previous paper extensively describes the test bench and the main obtained experimental results (Parthoens et al., 2021). The main inputs and outputs of this campaign are briefly recalled here.

The heat pump shows a conventional architecture, working with R134a fluid. Thermocouples, pressure sensors and mass flowmeters are installed on the test bench in order to monitor the fluid state at the boundary of each component. The evaporator shows a fins and tubes configuration. Its refrigerant loop is split into three distinct circuits with a separation on the height of the device. The mass accumulation of condensation and/or frost can be recorded using two different techniques (weight of the whole set up), while the outer metallic casing of the evaporator is replaced by transparent polymer material. It allows to have a partial visual control of the top of the exchanger. Pictures are taken every 30 seconds to have a visual representation of the frost thickness and distribution. The frost thickness is evaluated with an image post-treatment procedure implemented with the help of the software *ImageJ*.

Based on the observation recorded on this test bench, a simulation tool is implemented to predict time dependent performance of such a system, in frosting conditions.

3. MODEL DESCRIPTION

3.1 Heat exchanger modeling – general scheme

The evaporator consists in a 4-row tubes and fins heat exchanger. It has 12 tubes on its height split in 3 independent circuits. Based on experimental observations and how the frost appears on the exchanger, it has been decided to consider a tube-by-tube model. Indeed, frost appears sequentially on the different tubes. However, for a given one, the frost is rather uniform on its whole length. Each cell of the model corresponds to one tube and its corresponding fins, except for the refrigerant transitional tube where a moving boundary is imposed.

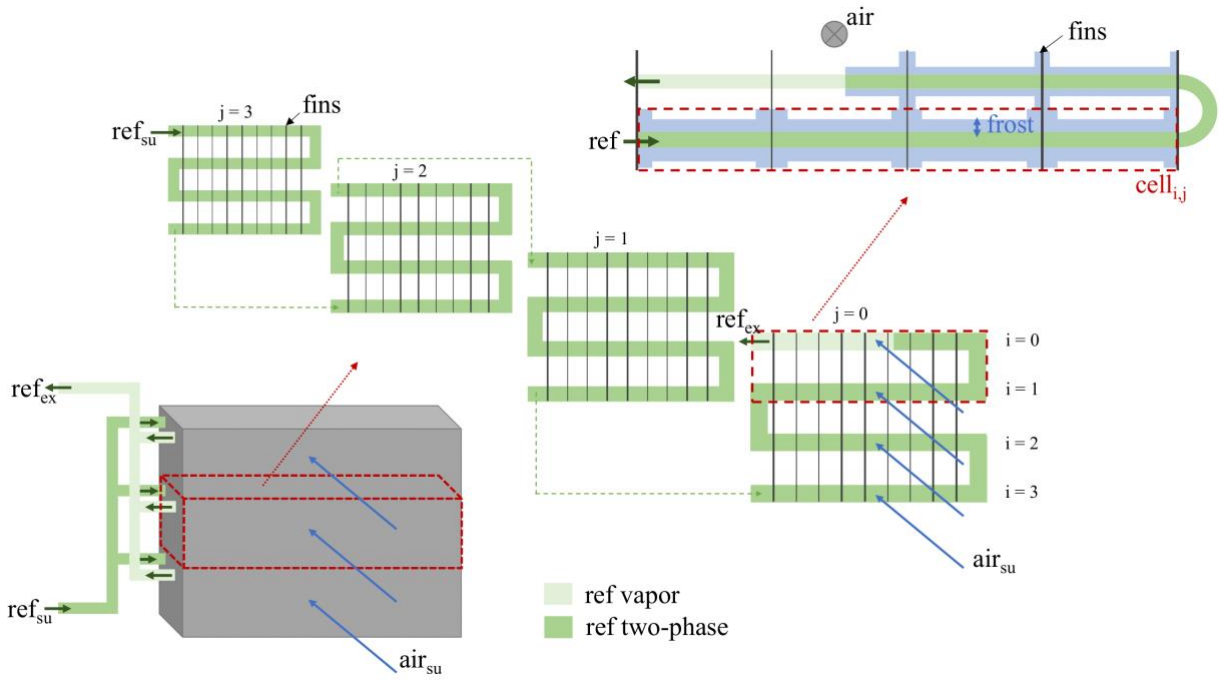

Figure 1 Geometry and control volume definition of the evaporator

To increase the robustness of the model, a dynamic approach has been selected. The main approach consists in considering a heat transfer between both working fluids and the wall (i.e. the tubes). At the beginning of the

simulation, the exchanger is considered equal to the ambient temperature. The air and refrigerant flows are exchanging a certain amount of energy due to the temperature difference. Cross fin conductive heat transfer is also implemented in the model. The user can either chose or not to account for this phenomenon in the simulations. The Section 3.4 is dedicated for this phenomenon due to its particular interest in the frame of this paper. The heat transfers rate computed on the airside $\dot{Q}_{air}$, on the refrigerant side $\dot{Q}_{ref}$ and through the fin $\dot{Q}_{Xfin}$ are computed based on heat transfer equations detailed in the next subsections. Following the obtention of those quantities, the wall temperature for the cell *i*, *j* is updated by means of:

$$m \cdot C \cdot \frac{d\,T_{wall,i,j}}{dt} = \dot{Q}_{ref,i,j} - \dot{Q}_{air,i,j} - \dot{Q}_{Xfin,i,j} \tag{1}$$

For a given cell, the wall temperature is considered uniform for the complete cell. The different heat transfer rate need to be computed. The general scheme allows to compute them independently, which decreases the global complexity of the model.

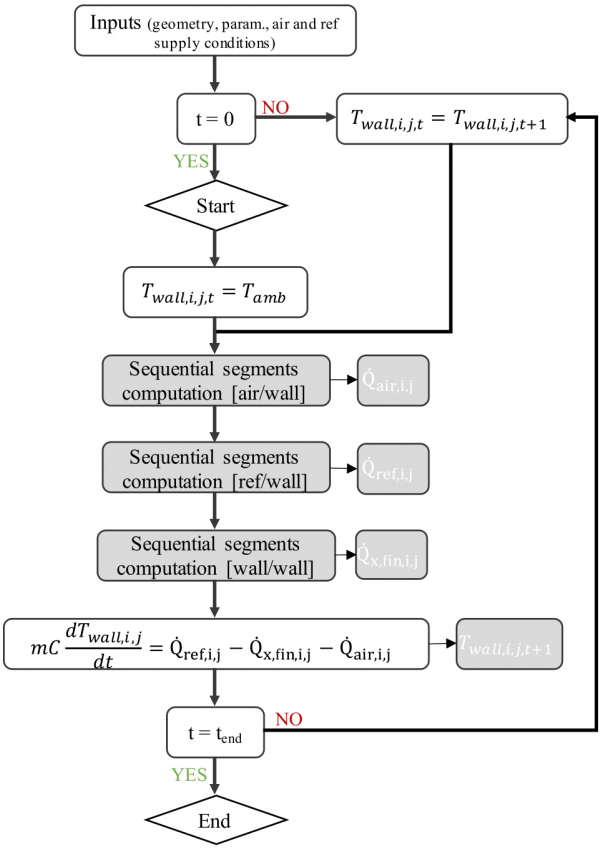

Figure 2 Exchanger algorithm flowchart

3.2 Heat exchanger modeling – refrigerant side

The resolution of the heat transfer between wall and refrigerant is rather classical. The solver runs each cell sequentially, beginning from the refrigerant supply to finish at the exhaust. The supply conditions of the cell *n* + 1 corresponds to the exhaust conditions of the cell *n*. As mentioned previously, each cell corresponds to a complete tube, except for the transition between two-phase and superheated phase. For each tube except one, the fluid is then either completely in two-phase or completely superheated.

Two-phase tube. While boiling, the refrigerant temperature is considered constant. It only depends on its pressure and considering a single tube, the pressure drops are small enough to neglect a temperature glide. This specific case corresponds to a heat transfer between two media at constant temperature. The classic heat transfer model is used.

$$\dot{Q}_{ref,i,j} = H_{ref,i,j} \cdot A_{ref,i,j} \cdot \left(T_{wall,i,j} - T_{ref,su,i,j}\right) \tag{2}$$

where $H_{ref,i,j}$ and $A_{ref,i,j}$ are the heat transfer coefficient and the exchange surface between wall and refrigerant, respectively.

Because of the exchanger geometry and more specifically the refrigerant split, the mass flux is relatively low, going from about 80 to 40 kg/m^2/s. Ma et al. (2020) conducted a study for smooth horizontal tubes for low mass fluxes. Different correlations from different authors are proposed and the one picked up for the model is the one from Kandlikar (1990). This choice is made because this model fits well, especially for very low mass fluxes. To describe refrigerant boiling, the correlation is based on two different contributions, namely the convective and nucleate boiling terms.

$$\frac{H_{ref,2P}}{H_{ref,L}} = C_1 \cdot Co^{C_2} \cdot (25 \cdot Fr_L)^{C_5} + C_3 \cdot Bo^{C_4} \cdot F_{fl} \quad (3)$$

where *Co* represents the convective number, *Bo* the boiling number, *Fr* the Froude number F_{fl} fluid dependent correction factor and C_i some constants. The convection number directly depends on the refrigerant quality, updated at the supply of each tube.

Superheated tube. In the superheated zone, the heat transfer between the refrigerant and the wall is a semi-isothermal heat transfer. The well-known ϵ-NTU methods is implemented to compute the heat exchange.

$$\dot{Q}_{ref,i,j} = \varepsilon \cdot \dot{C}_{ref} \cdot \left(T_{wall,i,j} - T_{ref,su,i,j}\right) \quad (4)$$

with

$$\varepsilon = 1 - \exp\left(-NTU_{ref}\right) \quad (5)$$

$$NTU_{ref} = \frac{AU_{ref}}{\dot{C}_{ref}} \quad (6)$$

$\dot{C}_{ref}$ being the refrigerant capacity flowrate in [W/K] and AU_{ref} the refrigerant overall heat transfer coefficient. To determine AU_{ref} the heat transfer coefficient $H_{ref,SH}$ is needed. It can be deduced from the well-known equation linking this coefficient to the Nusselt number:

$$H_{ref,SH} = \frac{Nu \cdot k}{D_h} \quad (7)$$

Nu is determined with the Dittus-Boelter equation from Incropera and Dewitt reference book (Bergman et al., 2011): if *Re* > 1e4:

$$Nu = 0.023 \cdot Re^{4/5} \cdot Pr^{0.4} \quad (8)$$

if *Re* <2300

$$Nu = 4.36 \quad (9)$$

and a weighted average of Equation (8) and (9) if *Re* is in between those values.

Transition. Transition tube corresponds to the tube in which the refrigerant exhaust specific enthalpy is greater than the vapor saturation specific enthalpy. When transition occurs, none of the method described before can be applied on its own. The objective is to find the proportion of the tube in two-phase state. The rate of heat transfer needed is easily deduced, knowing the saturation specific enthalpy:

$$\dot{Q}_{ref,i,j,part,2P} = \dot{M}_{ref} \cdot \left(h_{ref,sat} - h_{ref,su,i,j}\right) \quad (10)$$

Knowing $\dot{Q}_{ref,i,j,part,2P}$ the corresponding exchange surface (i.e. the proportion of the tube) can be deduced, rearranging Equation (2).

3.3 Heat exchanger modeling – air side

On the air side, for each tube, the ε-NTU is implemented. The only difference with the refrigerant side is the presence of fins, which was not the case on refrigerant side. It is expressed in the definition of the global heat transfer coefficient *AU*:

$$AU_{air} = (A_{tube} + A_{fins}) \cdot \eta_{surf} \cdot H_{air} \quad (11)$$

with η_{surf} being the surface efficiency. It penalizes the heat transfer coefficient to account for the fact that the complete surface is not at the wall temperature and is computed accordingly to VDI Heat Atlas (GmbH, 2010).
However, if the temperature of the surface is below the air dew point, additionally to heat transfer, there will be a mass transfer due to condensation or frost formation. The details of the models used here can be found in the works of Gendebien et al. (2013, 2019). It is to note that each cell/tube is considered as completely dry, wet or frosted.

3.4 Fin thermal conduction modeling

The fin thermal conduction impact is a phenomenon due to the temperature difference of two tubes, linked by metallic fins. The temperature difference creates a potential, leading to conduction heat transfer in the set of fins.

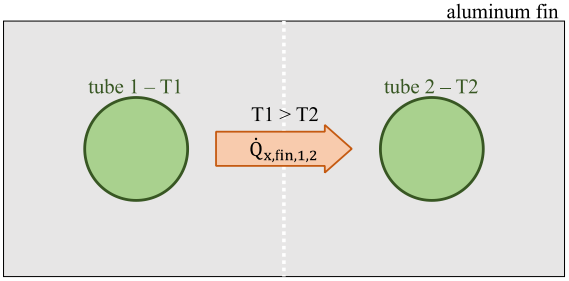

Figure 3 Cross fin thermal conduction illustration

Because it substantially increases the model complexity and computational cost (Sarfraz et al., 2019), fin conductivity is not often taken into account, especially when frost events occur. However, the frost distribution is tightly linked to the surface temperature. Fin thermal conductivity may have an impact on wall temperature when a tube with superheated refrigerant at around 15°C is very close by another tube where the refrigerant is at -7°C.

A reasonable assumption made is to only consider thermal conduction from one tube to its direct neighbors. A tube in the pack has a maximum of six neighbors, and less if the tube is located at the exchanger edge. Based on the conduction equation, the heat transfer through fins between two tubes can be expressed as :

$$\dot{Q}_{Xfin,i,j} = L_{fin,thick} \cdot D_{ext} \cdot N_{fin} \cdot k_{fin} \cdot \sum_{k=1}^{N} \frac{T_{wall,i,j} - T_{wall,k}}{d_k} \quad (12)$$

where N_{fin} is the number of fins, $T_{wall,k}$ is the wall temperature of the k^{th} direct neighbor of the tube i,j and d_k the distance between those tubes.

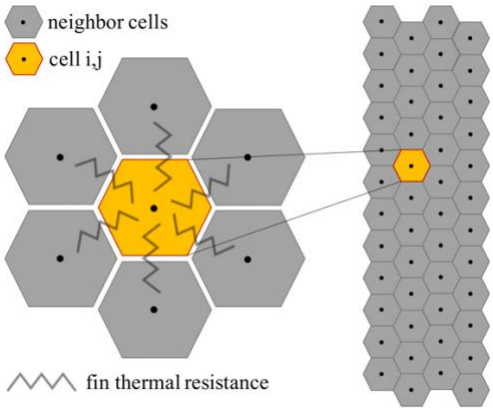

Figure 4 Exchanger staggered configuration (a black dot corresponds to a tube)

To solve those equations, all neighbors wall temperatures must be known in advance. Knowing that the resolution is sequential, considering a model in (quasi-)steady state would result in an additional set of N+1 additional iteration variables, leading to a poorly robust model. On the contrary, implementing a dynamic model with wall capacity allows to know the complete exchanger wall temperatures at a time t, without any additional iteration variable. This is possible

because the forward Euler method is adopted, allowing to compute the temperatures of time $t + 1$ at time t. The wall temperature of the cell i, j for the next time step is computed using Equation (1):

$$T_{wall,i,j,t+1} = T_{wall,i,j,t} + \frac{d\,t}{m \cdot C} \cdot \left(\dot{Q}_{ref,i,j} - \dot{Q}_{air,i,j} - \dot{Q}_{Xfin,i,j}\right) \tag{13}$$

4. MODEL VALIDATION

The simulated heating transfer rate is compared with the simulations in order to validate the model. On the air side, the dry, the wet and the frost regimes are envisaged individually. For the dry and wet ones, the different values are in steady state. For the frost regime, as conditions are perpetually evolving, different points at the beginning, middle and end of each test are displayed.

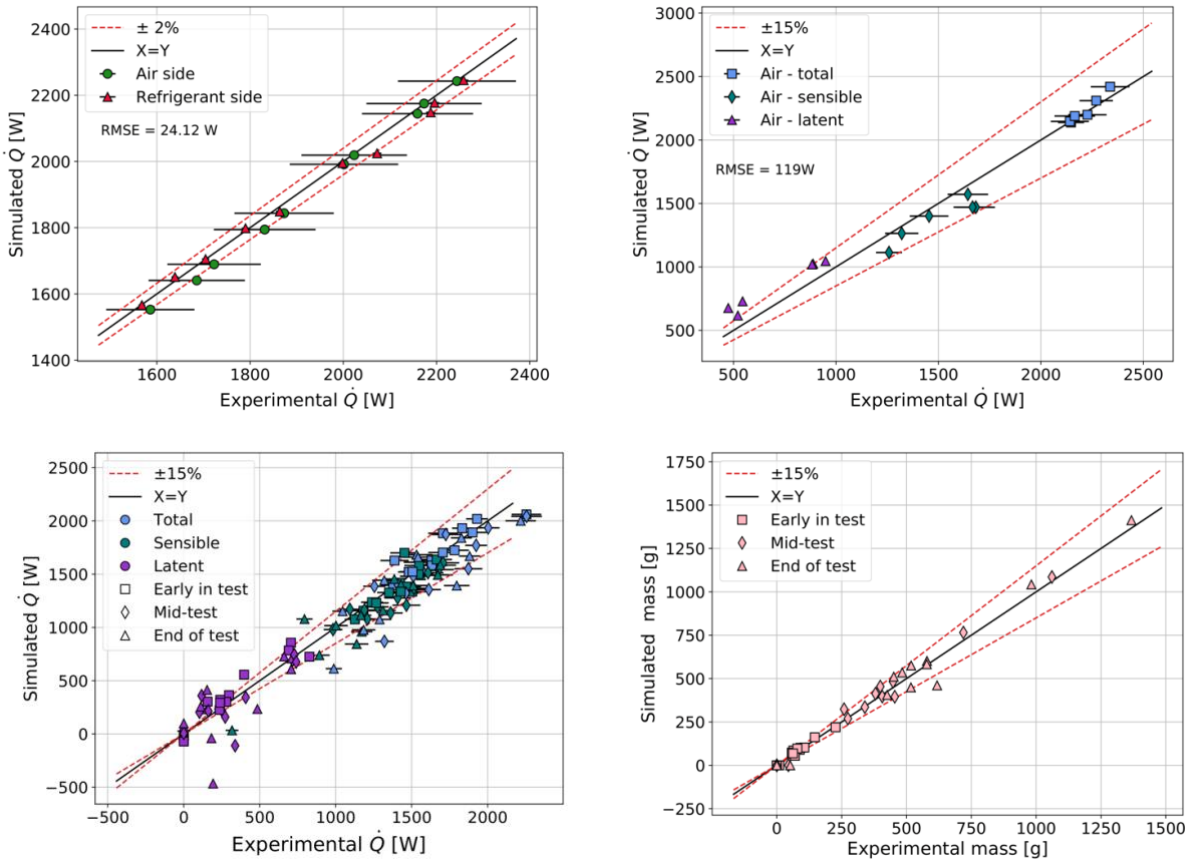

Figure 5 Experimental validation of the heat exchanger model : up-left, up-right and bottom-left correspond to dry, wet and frost regime, respectively. Bottom-right corresponds to the validation of the amount of water in frost regime.

Globally, the predicted results fit well and are within the 15% error compared to experimental measurements (with even better performance in dry regime). For the frost, no particular difference can be seen regarding the temporality of the tests, meaning that, with time running, no degradation of the prediction is to declare. Higher differences can be spotted, especially for the latent loads. They mainly correspond to end of test and disturbances that can occur at this time (e.g. valve hunting effects or compressor shut down).

After the study of these conventional quantities, an add-on of this paper is the study the frost distribution, regarding the impact of the fin thermal conductivity (FTC). The most relevant available experimental data is the frost thickness

extracted from pictures taken from the top of the evaporator during the test duration. First, to illustrate the FTC effect, pictures of a representative test is taken after 10, 60 and 90 minutes. These pictures are faced with a representation of the predicted frost thickness on each tube of the evaporator. The model is, at first, ignoring FTC effect, as it is the case in all previous works examined by the first author. Then, the exact same simulation is executed considering this effect. Those representations are found in Figure 6.

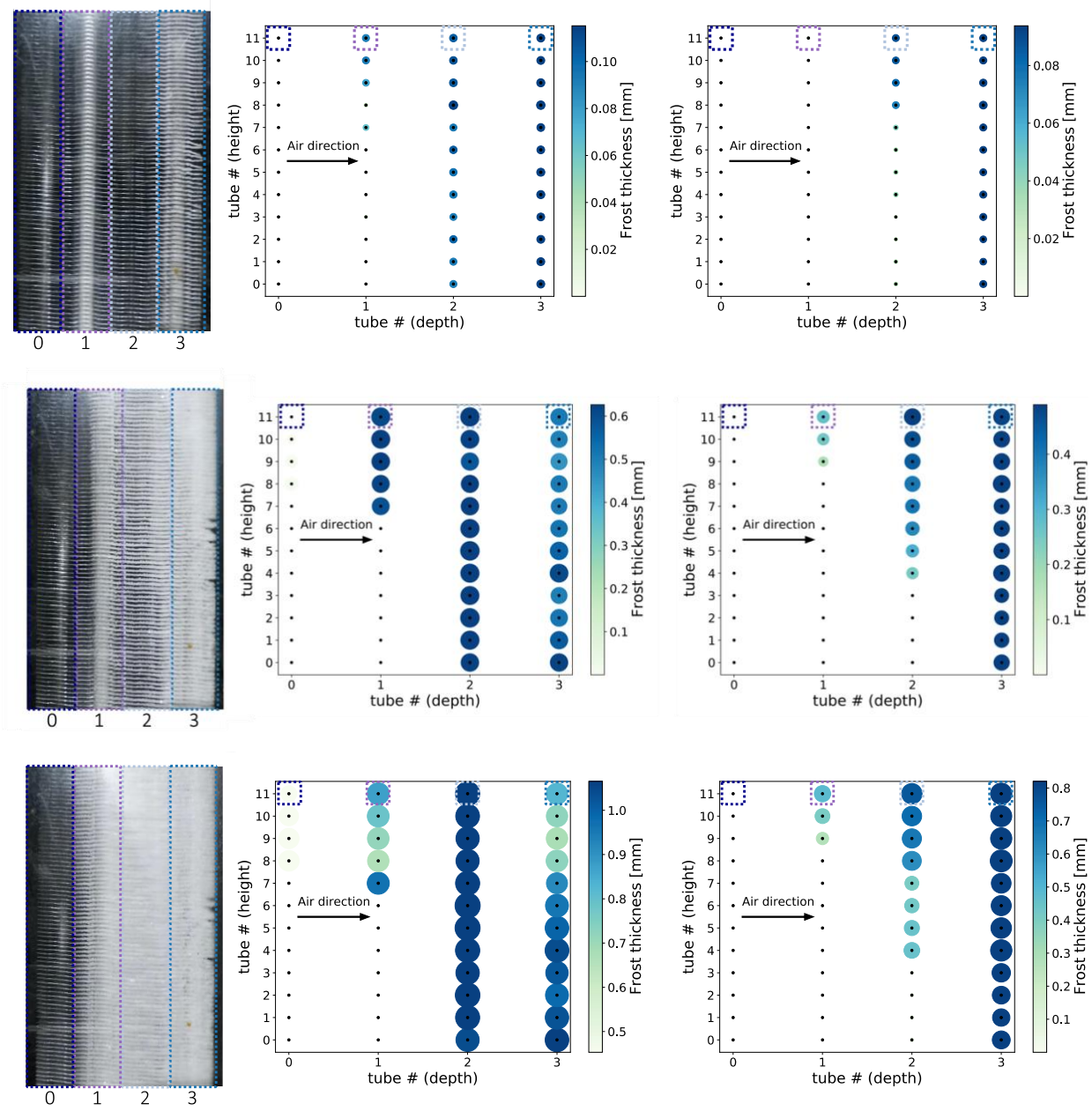

Figure 6 Frost distribution in the different tubes of the heat exchanger. From top to bottom, figures corresponds to 10, 60, 90 minutes, respectively. The left corresponds to the actual picture of the test, the **center** and *right*, to the model result **without** and *with* FTC, respectively

Figure 6 explicitly reveals the impact of this phenomenon. The first general comment is that there is an uneven distribution of frost on the exchanger height because of the unbalanced refrigerant split in its different loops. Then, the size of the circles is only qualitative and is not proportional compared to the exchanger geometry. This size is a good indicator to get a general view on the frost distribution while the colors bring more accuracy to the actual

thickness. Finally, all the tubes of the exchanger are represented. However, the visual access is only available on the top of the exchanger. Those are highlighted with colored boxes, in the pictures and in the simulation results.

Minute 10. Even if the difference is not striking, the picture explicitly shows frost on the middle blue tubes (Tube 3). At this stage, without thermal conductivity, frost already appears on three out of the four tubes. This effect is reduced thanks to the FTC.

Minute 60. The experimental data shows a more important quantity of frost at the middle blue tubes level. Then going backwards, this quantity decreases. Without FTC, the predictions differs with a larger quantity on the light blue and violet tubes. As no thermal transfer is accounted between tubes of different temperatures (over-heated and two-phase tubes), humidity from air frosts as it hits the first sub-zero tube. The air being dryer for the next tubes, the quantity of frost accumulated is smaller. Now, accounting for FTC, the superheated tube heats-up the next tubes. It increases the surface temperature of neighbor tubes, delaying the frost formation on the further tubes.

Minute 90. The analysis made for minute 60 is the same and even emphasized. Small amount of frost is predicted on the dark blue tube (Tube 0) without FTC, which is not observed on the experimental data.

The previous analysis focuses on three specific moments of the test and no quantitative comparison between the model predictions and the measurements is provided. To complete the analysis, the frost thickness is plotted as a function of the time, again, with and without taking into account the FTC effect.

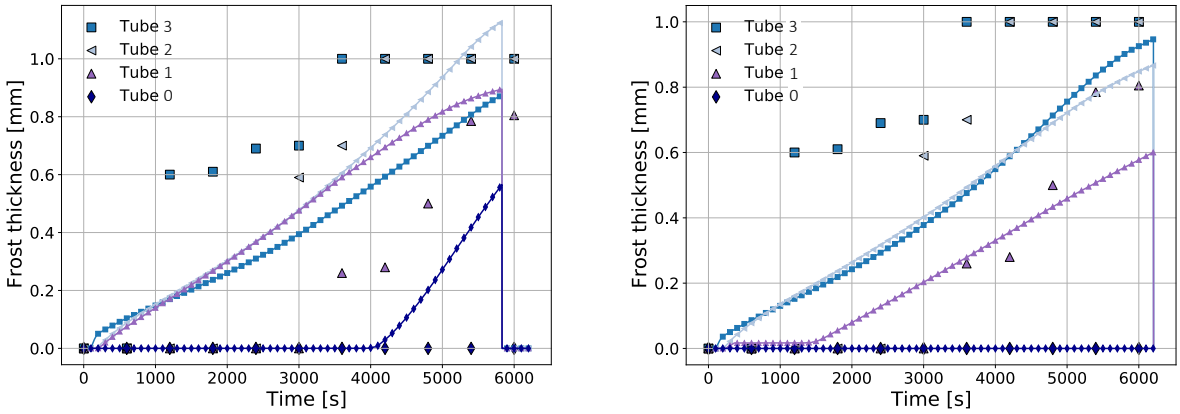

Figure 7 Experimental (discontinuous markers) and simulation (continuous lines) representations of temporal evolution of frost accretion on the four top tubes of the evaporator. Left figures does not account for FTC while the right does

The conclusions are the same as in the previous analysis. Tubes 1 and 2 dominate in terms of frost thickness over Tube 3 (light blue). Furthermore, a bad prediction of frost accretion on Tube 0 (dark blue). Even if the fit is still not perfect, a substantial correction is brought thanks to the FTC consideration. Looking at the numerical values, even in the best case, the match is not perfect. However, it should be recalled that the thickness is in tenth of millimeters and the experimental data comes from a picture analysis. This technique is efficient but may present a lack of accuracy, explaining the difference between the simulations and experiments.

To sum-up, this section shows that the novelty brought with the consideration of FTC is a real add-on in the frost formation simulation in heat exchangers. A bad frost distribution prediction due to the lack of FTC implies bad predictions in the pressure drop characterization and may have a serious impact on the design of heat exchangers.

5. CONCLUSIONS

This paper presents a new model of evaporator accounting for fin thermal conductivity. The conclusions are the following:

- Experimental data used to visualize frost and validate the presented model is available in another publication (Parthoens et al., 2021);

- The model is tube-by-tube discretised model, to account for frost uneven distribution in the device;
- Refrigerant and air and fin thermal conductions are decoupled. Each heat transfer rate is computed independently and briefly explained in this paper;
- The model is successfully experimentally validated regarding the heat transfer rate and mass accumulation in the evaporator;
- Regarding the frost distribution, it is clearly shown that fin thermal conductivity has a critical positive impact on the model prediction.

NOMENCLATURE

A	Surface area	(m^2)	**Subscript**	
Bo	Boiling number	(-)	2P	two-phase
$\dot{C}$	Capacity flowrate	(W/K)	ext	external
Co	Convective number	(-)	part	partial
D	Diameter	(m)	ref	refrigerant
F_{fl}	Fluid dpdt correction factor	(-)	SH	superheated
Fr	Froude number	(-)		
FTC	Fin Thermal Conductivity	(-)		
h	Specific enthalpy	(J/kg)		
H	Heat transfer coefficient	($W/m^2/K$)		
k	Thermal conductivity	(W/m/K)		
L	Length	(m)		
$\dot{M}$	Mass flowrate	(kg/s)		
Nu	Nusselt number	(-)		
$\dot{Q}$	Heat transfer rate	(W)		
Re	Reynolds number	(-)		
T	Temperature	(°C or K)		

REFERENCES

Jinchen Tang et al. (2020). Computational modeling and prediction of the performance of air source heat pumps under frost prevention and retardation conditions. *Energy and Buildings* 224 , 110264.

Hong Chen, Leena Thomas, and Robert W Besant (2003). Fan supplied heat exchanger fin performance under frosting conditions". In: *International Journal of Refrigeration* pp. 140–149.

YZPSY Xia et al. (2006) "Frost, defrost, and refrost and its impact on the air-side thermal-hydraulic performance of louvered-fin, flat-tube heat exchangers". In: *International Journal of Refrigeration* 29.7 , pp. 1066–1079.

Huee-Youl Ye and Kwan-Soo Lee (2013) "Performance prediction of a fin-and-tube heat exchanger considering air-flow reduction due to the frost accumulation". In: *International Journal of Heat and Mass Transfer* 67 pp. 225–233.

Dong-Keun Yang, Kwan-Soo Lee, and Simon Song (2006) "Modeling for predicting frosting behavior of a fin–tube heat exchanger". In: *International journal of heat and mass transfer* 49.7-8 , pp. 1472–1479.

Jin Woo Yoo et al. (2018) "Determination of defrosting start time in an air-to-air heat pump system by frost volume calculation method". In: *International Journal of Refrigeration* 96, pp. 169–178.

Diogo L Da Silva, Christian JL Hermes, and Claudio Melo (2011) "First-principles modeling of frost accumulation on fan-supplied tube-fin evaporators". In: *Applied Thermal Engineering* 31.14-15, pp. 2616–2621.

Haobo Jiang, Vikrant Aute, and Reinhard Radermacher (2006) "CoilDesigner: a general- purpose simulation and design tool for air-to-refrigerant heat exchangers". In: *International Journal of Refrigeration* 29.4, pp. 601–610.

Donghun Kim, James E Braun, and Sugirdhalakshmi Ramaraj (2018) "Computationally efficient modeling strategy for evaporator performance under frost conditions". In: *International Journal of Refrigeration* 96, pp. 88–99.

R Mastrullo et al. (2014) "Transient model of a vertical freezer with door openings and defrost effects". In: *Applied energy* 121, pp. 38–50.

A Morales-Fuentes et al. (2018) “Analysis of the heat transfer area distribution in a frosted plain fin-and-tube geometry”. In: *International Journal of Refrigeration* 75 pp. 26–37.

Yanping Xia and Anthony M Jacobi (2005) “Air-side data interpretation and performance analysis for heat exchangers with simultaneous heat and mass transfer: wet and frosted surfaces”. In: *International Journal of Heat and Mass Transfer* 48.25-26, pp. 5089–5102.

Jian Liu et al. (2004) “A general steady state mathematical model for fin-and-tube heat exchanger based on graph theory”. In: *International Journal of Refrigeration* 27.8, pp. 965–973.

Ricardo Romero-Méndez et al. (1997) “Effect of tube-to-tube conduction on plate-fin and tube heat exchanger performance”. In: *International journal of heat and mass transfer* 40.16, pp. 3909–3916.

Omer Sarfraz, Christian K Bach, and Craig R Bradshaw (2019) “Discrete modelling of fin-and-tube heat exchangers with cross-fin conduction functionality”. In: *International Journal of Refrigeration* 104, pp. 270–281.

Varun Singh, Vikrant Aute, and Reinhard Radermacher (2008) “Numerical approach for modeling air-to-refrigerant fin-and-tube heat exchanger with tube-to-tube heat transfer”. In: *International Journal of Refrigeration* 31.8, pp. 1414–1425.

Parthoens, A., Gendebien, S., & Lemort, V. (2021). Implementation of Innovative Measurement Techniques for Implementation of Innovative Measurement Techniques for Precise Experimental Characterization of Frost Growth in a Heat Pump Evaporator. *18th International Refrigeration and Air Conditioning Conference* . Purdue: Purdue e-Pubs.

Gendebien, S., Bertagnolio, S., & Lemort, V. (2013). Investigation on a ventilation heat recovery exchanger: Modeling and experimental validation in dry and partially wet conditions. *Energy and Buildings*, 176-189.

Gendebien, S., Parthoens, A., & Lemort, V. (2019). Investigation of a single room ventilation heat recovery exchanger under frosting conditions: Modeling, experimental validation and operating strategies evaluation. *Energy and Buildings*, 1-16.

Ma et. al, X. (2020). Condensation and Evaporation Heat Transfer Characteristics of Low Mass Fluxes in Horizontal Smooth Tube and Three-Dimensional Enhanced Tubes. *Journal of Thermal Science and Engineering Applications* .

Kandlikar, S. G. (1990). A general correlation for saturated two-phase flow boiling heat transfer inside horizontal and vertical tubes. *Journal of heat transfer*, 219-228.

Bergman, T., Lavine, A., Incropera, F., & DeWitt, D. (2011). *Introduction to Heat Transfer 6th Edition.* John Wiley & Sons.

Sarfraz, O., Bach, C., & Bradshow, C. (2019). Discrete modeling of fin-and-tube heat exchangers with cross-fin conduction functionality. *International Journal of Refrigeration*, 270-281.

GmbH, V.-V. (2010). *VDI Heat Atlas.* VDI-Verlag GmbH.

ACKNOWLEDGEMENT

Antoine Parthoens would like to thanks the Fund for Scientific Research of Belgium (F.R.S - F.N.R.S) for the financial support - Research fellowship *FC31853.*